HAL
archives-ouvertes.fr

The operational calibration of images taken in the visible channel of the Meteosat-series of satellites

Christelle Rigollier, Mireille Lefèvre, Philippe Blanc, Lucien Wald

▶ **To cite this version:**

Christelle Rigollier, Mireille Lefèvre, Philippe Blanc, Lucien Wald. The operational calibration of images taken in the visible channel of the Meteosat-series of satellites. Journal of Atmospheric and Oceanic Technology, American Meteorological Society, 2002, 19 (9), pp.1285-1293.

HAL Id: hal-00363675

https://hal.archives-ouvertes.fr/hal-00363675

Submitted on 24 Feb 2009

HAL is a multi-disciplinary open access archive for the deposit and dissemination of scientific research documents, whether they are published or not. The documents may come from teaching and research institutions in France or abroad, or from public or private research centers.

L'archive ouverte pluridisciplinaire **HAL**, est destinée au dépôt et à la diffusion de documents scientifiques de niveau recherche, publiés ou non, émanant des établissements d'enseignement et de recherche français ou étrangers, des laboratoires publics ou privés.

Rigollier C., Lefèvre M., Blanc Ph., Wald L., 2002. The operational calibration of images taken in the visible channel of the Meteosat-series of satellites. Journal of Atmospheric and Oceanic Technology, 19, 9, 1285-1293.

THE OPERATIONAL CALIBRATION OF IMAGES TAKEN IN THE VISIBLE CHANNEL OF THE METEOSAT-SERIES OF SATELLITES

Christelle RIGOLLIER, Mireille LEFEVRE, Philippe BLANC, Lucien WALD

Groupe Télédétection & Modélisation, Ecole des Mines de Paris

BP 207, 06904 Sophia Antipolis cedex, France

lucien.wald@ensmp.fr

Abstract

A method and its implementation are presented for the automatic calibration of the images taken in the visible channel of the Meteosat series of satellites. The method performs on a daily basis and is based on a statistical analysis of two images: one when the sun illuminates the entire field of view of Meteosat, the other during nighttime. This approach does not require any information about atmospheric and surface parameters, and therefore can be easily performed either on archived data, or in quasi-real time when receiving the images. Daily calibration coefficients were obtained since 1985 and are available on the Internet. The results are fully consistent with previous studies.

1. INTRODUCTION

The calibration function describes the relationship between the digital count and the actual geophysical value of the object seen. For example, when dealing with time-series of images for climate or global change studies, analyses are made of each image, including comparison between images. These images should be well calibrated with respect to each other, in order to ensure that any variation in time is due to change in the signal coming from the observed target, and not from a change in calibration of the observing system. This paper deals with the calibration of the visible channel of the Meteosat series of satellites. These satellites are geostationary and provide synoptic views of Europe, Africa, and the Atlantic Ocean for meteorological purposes every half hour in three channels: visible broadband, thermal infrared and middle infrared (Morgan 1978). They are nominally located over longitude 0°. Initiated by the European Space Agency (ESA), the program is currently operated by Eumetsat, an European agency comprising the national weather offices.

Table 1 displays the history of changes in the operational satellite in the Meteosat program, up to June 1998. A slot denotes the half-hour period necessary for the acquisition of an entire image. Slot 1 denotes the half hour between 0000 and 0030 UTC, slot 2: 0030 and 0100 UTC, and slot 48: 2330 and 2400 UTC. This table shows a large number of changes. The various Meteosat sensors have different sensitivities due to their difference in the spectral band. Each of the spectral channels can be operated at one of 16 different gain levels. These gain levels are used to obtained the optimum dynamic range for each spectral channel and are adjusted as required (Eumetsat, 1996). This occurred several times within the periods given in the table. These sub-periods are not reported in this table, though they are taken into account. These changes in gain affect the sensitivity of a given sensor, and are to be compensated by an adjustment of the operational calibration coefficient.

2. THE EARTH VIEWING CALIBRATION APPROACH

The satellites of the Meteosat series have no onboard calibration system in the visible range. Added to the lack of prelaunch calibration for some of the satellites, this prevents an accurate calibration of the digital outputs of the radiometers into accurate radiance measurements. The European Space Agency and Eumetsat performed from time to time perfectly calibrated airborne measurements (Kriebel 1981; Kriebel and Amann 1993; Kriebel *et al.* 1996), which permit the computation of accurate calibration coefficients for a limited period. The calibration coefficients of the visible channels are not dynamically adjusted within the Meteorological Products Extraction Facility (Eumetsat 1996). In its Web site (see online at *www.eumetsat.de*), Eumetsat proposes a series of calibration coefficients on a yearly basis.

This is far from being sufficient in our opinion, especially when looking at the numerous changes occurring each year (see Table 1). A higher temporal sampling is needed and daily calibration coefficients should be computed using the Earth viewing approach. This approach is based on the knowledge and modeling of physical characteristics of some Earth phenomena as well as upon the processing of the digital imagery flowing down from the sensor itself (Abel 1990; Frouin, Gautier 1987; Köpke 1982, 1983).

Several methods were proposed to calibrate the Meteosat images. They are based on the resolution of the equation of radiative transfer that requires knowledge of atmospheric and surface parameters (Brisson *et al.* 1990; Cabot *et al.* 1994; Govaerts *et al.* 1998; Köpke 1982, 1983; Moulin *et al.* 1996; Moulin, Schneider 1999). Another technique consists in comparing the counts from a radiometer with data from a similar calibrated radiometer carried by an aircraft or a satellite (Kriebel 1981; Kriebel, Amann 1993; Kriebel *et al.*

1996). This kind of calibration does not take into account the drift of the various Meteosat sensors over a long period, or their differences in spectral responses.

These methods have been extensively reviewed in Lefèvre *et al.* (2000). Their advantages and drawbacks are analyzed and discussed. Operating a method for the calibration of large time series of images, we found it difficult to implement the cited method in a processing chain, mostly because of the need of atmospheric (water vapor, ozone, aerosol optical properties) and surface parameters (e.g., temperature). The method recently proposed by Lefèvre *et al.* (2000) , also called the autocalibration method, offers the advantage of being entirely automatic, and is the only automatic one to our knowledge. It has been proved as accurate as others using sophisticated modeling of the optical properties of the atmosphere and of the reflection properties of selected objects on the ground, such as deserts or oceans. Accordingly, we selected this method for an operational implementation.

3. THE AUTO-CALIBRATION METHOD

This method is based on the analysis of two quantities that are constant in radiance over the time series. These quantities are statistical parameters using the fact that in the entire field of view of the Meteosat sensor which covers approximately one-third of the Earth, the mixed presence of land, ocean, and clouds of different reflectivity, whatever the day and time of the year, leads to the preservation of such statistical quantities with time. In an empirical way, three parameters were selected by Lefèvre *et al.* that are the numerical counts *CN* corresponding to a dark target, and to the percentiles 5 % and 80 % of the histogram of the midday image. These numerical counts vary in time according to the Meteosat sensor and the date of viewing, but the two quantities that are derived in radiances (and defined in the following) were found constant for the test periods. Then it was hypothesized that any drift in these quantities should reflect a drift in the calibration of

the Meteosat sensor for any period of time. Lefèvre *et al*. demonstrated *a posteriori* the validity of this assumption by the very good results obtained in calibration when compared to other published works. Nevertheless, Lefèvre *et al.* recognized the heuristic aspect of the approach. They stressed that only the percentiles 5 % and 80 % offer such invariance, while one may expect a greater stability in the selection of the percentiles.

Assuming a linear response of the sensor, the relationship between the emerging radiance from the atmosphere and measured by the sensor, L^t, and the numerical count, CN^t, observed at instant t is

$$L^t = \alpha^t (CN^t - CN0^t) \qquad (1)$$

where α^t and $CN0^t$ are, respectively, the calibration coefficient of the sensor (in W m^{-2} sr^{-1} CN^{-1}) and the offset numerical count of the calibration.

Actually, the autocalibration method can only perform on an image relative to another. To calibrate a series of images, the procedure is the following:

- use a calibration function found in the literature,
- calibrate the image corresponding to that day (called hereafter the reference image), and
- perform the autocalibration method to calibrate all the other images relative to the reference one.

The first two steps are performed only once. Once the calibration function selected for the reference day t_0, *i.e.* α^{t0} and $CN0^{t0}$, this function is applied to the corresponding images for this day noted t_0, using Eq. 1.

The percentiles 5 % and 80 % of the mid-day image, when most of the field of view is illuminated, correspond to the numerical counts, respectively, CN^t_5 and CN^t_{80}, for which 5 percent (respectively 80 %) of the surface of the cumulative histogram is reached (percentile 5 %, respectively 80 %). The third parameter of interest is the numerical count

CN^t_{dark} of a dark target, namely the first mode of the histogram of an image acquired at a night slot, when approximately half of the field of view is in the dark.

According to Eq. 1, the radiances corresponding to the numerical counts CN^t_5, CN^t_{80} and CN^t_{dark} are given by:

$$L^t_{dark} = \alpha^t (CN^t_{dark} - CN0^t)$$

$$L^t_5 = \alpha^t (CN^t_5 - CN0^t) \qquad (2)$$

$$L^t_{80} = \alpha^t (CN^t_{80} - CN0^t)$$

It becomes:

$$\alpha^t = (L^t_{80} - L^t_5) / (CN^t_{80} - CN^t_5) \qquad (3)$$

$$CN0^t = CN^t_{dark} - L^t_{dark} (1/\alpha^t)$$

Note that F^t is the incoming extraterrestrial solar irradiance in the visible channel for the Meteosat sensor under concern. If I_{0met} is the total irradiance in the visible channel, that is $I_{0met} = \int_{0.3}^{1.1} I_{0\lambda} S_\lambda \, d\lambda$, with S_λ being the sensor spectral response in the visible range, covering approximately the interval [0.3 μm, 1.1 μm] for Meteosat, and if $\varepsilon(t)$ is the eccentricity of the Earth orbit, then $F^t = I_{0met}(t) \, \varepsilon(t)$.

Lefèvre *et al.* found two quantities that are invariant in time. The first quantity expresses that the most frequent radiance observed by the sensor when looking at the obscurity towards the Earth is time invariant:

$$L^{t0}_{dark} / I_{0met}(t_0) = L^t_{dark} / I_{0met}(t) \qquad (4)$$

Actually, one mistake was made in the original article: the eccentricity $\varepsilon(t)$ should not intervene in this quantity. Equation 4 is the correct version.

The second quantity deals with the images of the Earth well illuminated by the Sun; the mixed presence of land, ocean, and clouds of different reflectivity over approximately one third of the Earth, whatever the day and time of the year, leads to the preservation of the dynamics of the observed signal. A first-order correction was brought to the original

equation of Lefèvre *et al.* We divided the quantity by the cosine of the solar zenith angle to avoid an unwanted period in signal of half a year. Noting the latitude and longitude of the center of the field of view Φ and λ (here, equal to zero), the invariant is then

$$(L^{t0}_{80} - L^{t0}_{5}) / F^{t0} \cos(\theta_S)_{t0,\ \Phi=0,\ \lambda=0} = (L^{t}_{80} - L^{t}_{5}) / F^{t} \cos(\theta_S)_{t,\ \Phi=0,\ \lambda=0} \qquad (5)$$

with

$$\cos\theta_S = \sin\Phi \sin\delta + \cos\Phi \cos\delta \cos\omega$$

where ω is the solar hour angle and δ is the declination for the day under concern. In both equations, the ratioing by $I_{0met}(t)$ or F^t accommodates for the changes in sensor, and thus of S_λ.

The calibration function of the autocalibration method is

$$L^t = a^t (CN^t - CN^t_{dark}) + b^t \qquad (6)$$

with

$$a^t = [(L^{t0}_{80} - L^{t0}_{5}) / (CN^t_{80} - CN^t_{5})]\ F^t \cos(\theta_S)_{t,\ \Phi=0,\ \lambda=0} / F^{t0} \cos(\theta_S)_{t0,\ \Phi=0,\ \lambda=0}$$

$$b^t = L^{t0}_{dark}\ I_{0met}(t) / I_{0met}(t_0)$$

The reference day was selected as $t_0 = 1$ *January 1985*. Lefèvre *et al.* demonstrated that the selection of the reference date has a negligible impact on the results. The calibration law for this reference date is that of Moulin *et al.* (1996):

$$L^{t0}_{dark} = 0{,}97\ (CN^{t0}_{dark} - 1{,}87) \qquad (7)$$

$$L^{t0}_{80} - L^{t0}_{5} = 0{,}97\ (CN^{t0}_{80} - CN^{t0}_{5})$$

The calibration law depends on the shape of the spectral sensitivity curve of the radiometer, S_λ. We adopt those used by Lefèvre *et al.* only for Meteosat-1 to -4 and those recommended by Govaerts (1999, see online at *www.eumetsat.de*) for Meteosat-5, -6 and -7. This is a large departure from the initial method, which results into a relative change in calibrated radiances of approximately 20 percent for these satellites. The total irradiances in the visible channel for the various Meteosat sensors, I_{0met}, are given in the table 2.

5. SELECTION OF SLOTS

The Meteosat data are available in full spatial resolution and also in reduced resolution. This reduced B2 format has been set up in the framework of the International Satellite Cloud Climatology Project (ISCCP; Schiffer, Rossow 1983, 1985), part of the World Climate Research Program (WCRP). The B2 set is produced by Eumetsat according to the following steps:

- first, time sampling of geostationary images reduces the frequency of observation to synoptic 3-h intervals, starting at 0000 UTC;
- second, the higher-resolution visible-channel data are averaged to match the lower resolution of infrared-channel data (*i.e.* an image of 2500 x 2500 pixels with a resolution of 5 km);
- third, overlapping image pixels are removed;
- fourth, spatial sampling of images is performed to reduce the resolution to approximately 30 km at nadir (*i.e.* a B2 image of 416 x 416 pixels with a resolution of 30 km), by taking 1 pixel in 6 in each direction. The value of the corresponding B2 pixel is given by the radiance of the southeasternmost pixel in a 6 x 6 pixels square.

The satellite measurements are, in all other respects, preserved in the reduced-resolution dataset, since volume reduction is accomplished by the sampling described above. Therefore, the calibration method can be applied to the B2 data without change.

The method is based on the analysis of two specific images: one acquired when the observed portion of the Earth is mostly in the obscurity of night and the other one when this portion is entirely illuminated. Slot 11 (0530 UTC) is used to compute CN^t_{dark} and the slot 24 (1130 UTC) to compute ($L^t_{80} - L^t_5$). These slots are not necessarily available in the whole time-series. Can another slot be used in such cases?

Figure 1 exhibits the series of images available in the B2 format on the 11 June 1996. One sees the variation in illumination of the portion of the Earth observed by the Meteosat satellite, located above the equator at longitude 0° (Gulf of Guinea). Before 16 November 1995, five slots only are supplied in the B2 format: slots 11, 17, 23, 29, and 35. After this date, eight slots are available: slots 6, 12, 18, 24, 30, 36, 42, and 48. After 2 October 1996, the slot 23 replaces the slot 24. When a slot has not been acquired correctly, Eumetsat replaces it by the closest slot offering a good quality if possible. During the quality check of each image performed at Ecole des Mines de Paris, some slots have been rejected, creating gaps in the time series.

The well-illuminated image is that of slot 23 (1100 - 1130 UTC) or 24 (1130 - 1200 UTC). Figure 1 clearly shows that the images for the slots before (17 or 18) and after (29 or 30) have obscure parts, which will bias the computation of the percentiles. For these images, the quantity $[(L^t_{80} - L^t_5) / F^t \cos(\theta_S)_{t,\, \varphi=0,\, \lambda=0}]$ is less invariant in time than for slot 23. In addition, changes of slot result in different viewing geometrical conditions that add to the uncertainties of the assessment. Accordingly, one should use as much as possible slots 23 or 24 for the calibration, or the neighboring slots from 21 to 26. If these slots are not available, the calibration should not be performed for this day, resulting in a gap in the time series.

As for the night slot, we analyzed the possibility of using slots 6, 42, or 48, when the field of view is entirely or almost entirely in obscurity. The results lead to calibrated values that are overestimated by a large amount compared to those obtained by Lefèvre *et al.*, Kriebel, Amman (1993) and Moulin *et al.* (1996). Accordingly, one should use as much as possible slots 11 or 12 for the calibration, or slots 35 or 36, whose images are symmetrical to those of slots 11 and 12. If these slots are not available, the image of slot 11 (or 12) of the day before can be used.

6. VARIABILITY OF THE PARAMETER a^t AND FILTERING

Figure 2 displays the time series of the coefficient a^t (Eq. 6), spanning from 1985 to 1997. A large variability in time appears and some periods may be detected. These observations are illustrated by the Fourier transform of this time series. The number of samples is 4543, the sampling time is 1 day and the cutoff frequency F_e is equal to 1 day^{-1}. Figure 3 displays the module of the Fourier transform for the interval [0, $0.01F_e$] (*i.e.* [100, 4543] in day). The peak corresponding to the mean value was removed but the influence of this mean value is still visible through the leftmost peak at 4098 days. Two other major peaks appear at 1170 and 819 days (frequencies close to 0.001 day^{-1}). These peaks, as well as the others, are due to changes of satellites and properties of radiometers. Analysis of Table 1 reveals very rapid changes in operating radiometers as well as large periods of time when the operating radiometer remains the same.

In this figure, the coefficient a^t computed from the original work of Lefèvre *et al.* is shown as a dotted line. The efficiency of the correction to remove the periods around 180 days (half year, frequencies close to 0.006 day^{-1}) is striking. The Fourier module confirms the large variability of the estimates of a^t in time.

At high frequencies, larger than $0.01F_e$, the signal a^t may be considered noise and consequently should be filtered out to produce a time series for operational use. The standard deviation of noise is not easy to determine. Two methods were employed. On one hand, following the work of Wald (1989) for other sensors, the variogram of the signal, also called the structure function, was analyzed, especially for the nugget effect. On the other hand, a wavelet transform of the signal provides the highest frequencies of the signal, which are assumed here to be only noise (Blanc 1999). Both methods give similar estimates of the standard deviation: 0.013 and 0.011 W m^{-2} sr^{-1} CN^{-1}, respectively.

The quantification step has also been assessed (Rigollier 2000). Two cases were studied: before and after 19 June 1989. Before this date, the quantification was made using six bits, while after eight bits were used. The corresponding standard deviation is 0.006 before 19 June 1989, and 0.003 W m^{-2} sr^{-1} CN^{-1} after this date. This standard deviation explains a large amount of the standard deviation of the noise (between 30% and 60%).

These various estimates of the noise permit the construction of the appropriate filter to remove the noise. The cutoff frequency is 0.09 day^{-1}, which is a period of 11 days. Hence, any variations in time less than 11 days will not be taken into account. A filter was synthesized by the apodization of Hemming; it comprises 33 coefficients *h(i)*, applying to the day *d-16* to the day *d+16* where *d* denotes the day under concern. The following relationships define the filtered signal a^{*t}:

$$a^{*t} = \sum_{i=-16}^{i=+16} a^{t-i}\, h(i) \qquad (8)$$

where

$$\sum_{i=-16}^{i=+16} h(i) = 1$$

The standard deviation of the differences between the original and the filtered signals is equal to 0.014 W m^{-2} sr^{-1} CN^{-1}. This value is slightly larger than the standard deviations of the noise previously assessed. The filtering reduces some of the variations in high frequencies in a^{*t}, which leads to a slight decrease of the standard deviation compared to the initial series of a^{t}.

7. OPERATIONAL IMPLEMENTATION

Eqs 2 - 6 are applied to the series of images spanning the period from 1985 to 1997. Several images are missing thus 4543 days (*i.e.* 9086 images) are processed. Each image of the time series was visually scrutinized for quality; the rejection of some images of

insufficient quality is the main cause of gaps in the time series. A series of calibration coefficients is obtained: CN^t_{dark}, b^t and a^t. The visual analysis of the series of the parameters CN^t_{dark}, b^t and a^t drawn as a function of the day provided an efficient means for detecting anomalies in quality that escaped the first screening. These days are removed from the time series. The gaps are filled by the interpolation of the three coefficients, using the known values for the days before and after the gap. The number of days used for interpolation is of little importance, given the filter to be applied later, except if the gap is larger than 11 days.

Changes in radiometers usually occur within the same day around 0800 UTC (Table 1). In this case, one cannot use the image of the early slot 11 (0500-0530 UTC) and the midday image to compute the calibration coefficients since they were not acquired by the same sensor. In principle, two sets of coefficients should be computed for such days: one before the change and one after. However, for the sake of the simplicity in the management of the calibration database and in the presentation of the calibration coefficients to the customer, we decided to compute only one set per day. This set corresponds to the midday image. The night slot is taken closest to this midday image: either slot 35 (or neighbors) of the same day, or slot 11 (or neighbors) of the day after.

Then the coefficient a^t is filtered to produce the series of a^{*t} (Eq. 8). To cope with the changes in radiometers, the filter is applied period after period, the radiometer and its gain configuration being constant within a given period. The mirror technique in filtering is used for the limits of the time interval.

Figure 4 displays the time series of the coefficients a^{*t}. One may note an abrupt change in a^{*t} for the day 1400 approximately, which denotes a change in gain configuration for the radiometer of Meteosat-2. Other abrupt changes are also visible for other satellites (e.g.,

Meteosat-3 and -4). This figure clearly shows rapid fluctuations of the coefficients, which induce the same variability of the radiance for the same numerical count.

Variability of such a magnitude is not reported in the literature. Eplee *et al*. (2000) and Barnes *et al.* (2001a) report short term variability in the observations of the lunar measurements for the calibration of the Sea-viewing Wide Field-of-view Sensor (SeaWiFS). Observations are made approximately once a month; the changes in calibration values exhibit a period of one year and the amplitudes in change are much lower than those observed in Fig. 4. These changes are caused by the annual cycle in the temperature of the SeaWiFS focal planes, which are warmest near the winter solstice and coldest near the summer solstice. The authors also mention that changes may occur by decreases in the quantum efficiencies of the photodiodes from exposure to infrared radiation in orbit. Barnes *et al.* (2000a) observe transitions in the instrument-diffuser sensitivity during eight days for this radiometer that are not explained. The radiometer CZCS experienced abrupt changes in calibration that were mostly due to outgassing. Evans, Gordon (1994) report a time scale of two weeks for short term variations.

The fluctuations observed in Fig. 4 likely indicate approximations in the retrieval method. Such fluctuations may be observed in the figures of Lefèvre *et al.* The time invariants are subject to the invariance, in a statistical sense, of the reflectivities offered by the mixed presence of land, ocean, and clouds over approximately one-third of the Earth. Obviously, the statistical distribution of the reflectivities fluctuates from day to day and it is believed that this is the main cause of the observed variability. However, given the published documentation reported above, we cannot exclude the possibility that some of the fluctuations originate from the radiometer itself.

8. COMPARISON WITH OTHER ESTIMATES OF THE CALIBRATION COEFFICIENTS

The results of this operational implementation were compared to published estimates of the calibration law. Three concurrent laws were identified. One is made of analytical formulas for assessing daily sets of calibration coefficients. The second one is an ensemble of monthly sets of calibration coefficients (*i.e.* one set per month). Finally, Eumetsat supplies yearly sets of calibration coefficients on its web site.

For each case, the comparison was performed on the time series of radiances that are computed by the various methods using an initial numerical count *CN=100*. The monthly or yearly values are duplicated to lead to daily values. In these two cases, the correlation coefficient does not have any significance. Table 3 reports some statistics of the comparison between our results and the others.

The study of Moulin and Schneider (1999) completes the initial study of Moulin *et al.* (1996), providing analytical formulae for assessing daily sets of calibration coefficients from 1 June 1983 (Meteosat-2) to 14 February 1997 (Meteosat-5). Moulin, Schneider make use of the early estimates of the spectral sensitivity curves for Meteosat-5, -6 and -7, and not those recommended by Govaerts (1999). This leads to an under-estimation of their retrieved radiances by approximately 20%. Accordingly, the comparison was only performed for the Meteosat-2 to -4 satellites. Both methods give similar results, as already noted by Lefèvre *et al*. The bias is negligible and the root-mean-square error (rmse) is low, less than the errors reported by Moulin *et al.* (13% in relative value). The correlation coefficient is large. If linear regression were to be made on our estimates to produce analytical formulas, the results would be very similar to those of Moulin *et al.*

Rossow *et al*. (1992), Desormeaux *et al*. (1993), Brest *et al.* (1997) and Rossow *et al.* (1995) describe the method developed for the ISCCP project. The ISCCP method is based

upon the comparison of reflectances measured by various sensors, including the Meteosat series, and by NOAA AVHRR-9 (NOAA-7 in the early publications). For the same reasons as above, the comparison is limited to the series Meteosat-2 to -4, which contains 1942 samples. The ISCCP method provides monthly sets of calibration coefficients. The estimated radiances are greater than ours for Meteosat-2, similar to ours for the initial period of Meteosat-3 and less than ours for the remaining days of the comparison. The relative bias amounts to 6 % and the relative rmse to 16 %. The ISCCP method agrees with ours, even if the results of the comparison are less successful than with the other methods. Indeed, it is difficult to reach precisely conclusions about this comparison as we were unable to find other sources of information confirming the results of this method, which is rather complex and contains several heuristic aspects.

Govaerts *et al.* (1998) base their calibration monitoring upon the simulation of the radiances at the top of the atmosphere over specific earth targets such as deserts. The calibration coefficients are computed for each year and are available on the Eumetsat web site (*www.eumetsat.de*). The comparison of the radiances thus calculated with ours is performed for the years 1995- 1997 (1089 samples). The yearly values cannot reproduce the observed variations neither the changes of radiometers that occur in this period (Meteosat-5, then Meteosat-6, again Meteosat-5 and Meteosat-6). The radiances calculated with the coefficients of Govaerts *et al.* are most often greater than ours. Nevertheless, the bias is small (5 % in relative value) as is the rmse (6 % in relative value). We may conclude that as a whole both methods agree.

9. CONCLUSIONS

An operational method has been implemented, tested, and validated for the calibration of the visible channel of the series of satellites of the Meteosat Operational Programme. It

performs on an automatic basis and is well suited for the processing of large volume of data.

Daily sets of calibration coefficients are obtained by this method, compared to the monthly or yearly sets given by some methods or to the approximated analytical laws of others. The present work results in a time series of daily sets for the years 1985-97, which constitutes a unique database. This database should be extended onward in the near future. Efforts were made to disseminate this database to the public through the Web site (*www.helioclim.net*). This site comprises also a history of the Meteosat sensors. To our knowledge, this developed service is unique in the world.

10. ACKNOWLEDGMENTS

This study was performed under the auspices of the European Commission in the framework of the project "SoDa: Integration and exploitation of networked Solar radiation Databases for environment monitoring," IST-1999-12245. Very fruitful discussions have been held with Eumetsat on several aspects: we particularly thank Yves Govaerts, for his help in the calibration activities and Richard Francis and the Archives Department MARF for providing the B2 data at no or low cost and for helping us in better understanding the Meteosat system and the properties of the B2 format. We thank the reviewers who made very valuable comments and greatly helped to increase the clarity of this article.

11. REFERENCES

Abel, P., 1990: Report of the workshop on radiometric calibration of satellite sensors of reflected solar radiation. March 27-28, 1990, Camp Springs, Maryland. NOAA Technical Report NESDIS 55, 33 pp.

Barnes, R. A., Eplee, R. E., Biggar, S. F., Thome, K. J., Zalewski, E. F., Slater, P. N., and A. W. Holmes, 2000a: SeaWiFS transfer-to-orbit experiment. *Appl. Optics*, 39(30), 5620-5631.

Barnes, R. A., Eplee, R. E., Robinson, W. D., Schmidt, G. M., Patt, F. S., Bailey, S. W., Wang, M., and C. R. McClain, 2000b: The calibration of SeaWiFS on orbit. *In* Earth Observing Systems V, W.L. Barnes Editor, Proceedings of SPIE, vol. 4135, 281-293.

Blanc, P., 1999: Développement de méthodes pour la détection de changement. Thèse de Doctorat, Ecole des Mines de Paris, Paris, France, 204 p.

Brest, C. L., Rossow, W. B., and M. Roiter, 1997: Update of radiance calibrations for ISCCP. *J. Atmos. Ocean. Tech.*, **14**, 1091-1109.

Brisson, A., Le Borgne, P., and A. Marsouin, 1990: Relative calibration of Meteosat visible radiometers. In Proceedings of the 8th Meteosat Scientific Users' Meeting, EUM P 08, Norrköping, Sweden, Published by Eumetsat, Darmstadt, Germany, 39-43.

Cabot, F., Dedieu, G., and P. Maisongrande, 1994: Monitoring NOAA/AVHRR and Meteosat shortwave bands calibration and intercalibration over stable areas. In Proceedings of the 6th ISPRS Symposium "Physical Measurements and Signatures in Remote Sensing", Vald d'Isère, France, Published by Centre National d'Etudes Spatiales, Toulouse, France, 41-46.

Desormeaux, Y., Rossow, W. B., Brest, C. L., and G. G. Campbell, 1993: Normalization and calibration of geostationary satellite radiances for ISCCP. *Journal of Atmospheric and Oceanic Technology*, **10**, 304-325.

Eplee, R. E., Barnes, R. A., Robinson, W. D., Bailey, S. W., Werdell, P. J., Patt, F. S., and C. R. McClain, 2000: SeaWiFS Calibration: Status after two years on orbit. *Journal of Atmospheric and Oceanic Technology*, **17**, 3163-3165.

Eumetsat, 1996: Annex to the Meteosat-5 calibration report. Meteorological Products Extraction Facility (MPEF), March 1996, Published by Eumetsat, Darmstadt, Germany, 25 pp.

Evans, R. H., and H. R. Gordon, 1994: Coastal zone color scanner "system calibration": a retrospective examination. *J. Geophys. Res.*, **99**, 7293-7307.

Frouin, R., and C. Gautier, 1987: Calibration of NOAA-7 AVHRR, GOES-5 and GOES-6 VISSR/VAS solar channels. *Remote Sensing Env.*, **22**, 73-101.

Govaerts, Y. M., 1999: Correction of the Meteosat-5 and –6 radiometer solar channel spectral response with the Meteosat-7 sensor spectral characteristics. *Int. J. Remote Sensing*, **20**, 3677-3682.

Govaerts, Y. M., Pinty, B., Verstraete, M. M., and J. Schmetz, 1998: Exploitation of angular signatures to calibrate geostationary satellite solar channels. *In* Proceedings of the IGARSS'98 conference, 6-10 juillet 1998, Seattle, USA, IEEE Catalog Number 98CH36174, **1**, 327-329.

Köpke, P., 1982: Vicarious satellite calibration in the solar spectral range by means of calculated radiances and its application to Meteosat. *Appl. Optics*, **21**, 2845-2854.

Köpke, P., 1983: Calibration of the Vis-channel of Meteosat-2. *Adv. Space Res.*, **2**, 93-96.

Kriebel, K.T., 1981: Calibration of the Meteosat visible channel by airborne measurements. *Appl. Optics*, **20**,11-12.

Kriebel, K. T., and V. Amann, 1993: Vicarious calibration of the Meteosat visible channel. *J. Atmos. Ocean. Tech.*, **10**, 225-232.

Kriebel, K. T., Mannstein, H., and V. Amann, 1996: Absolute calibration of the Meteosat-5 visible channels. In Proceedings of the 1996 Meteorological Satellite Data Users' Conference, EUM P 19, Published by Eumetsat, Darmstadt (Germany), pp. 31-40.

Lefèvre, M., Bauer, O., Iehlé, A., and L. Wald, 2000: An automatic method for the calibration of time-series of Meteosat images. *Int. J. Remote Sensing*, **21**, 1025-1045.

Morgan, J., 1978: Introduction to the Meteosat system, ESOC, European Space Agency (ESA), 54 pp.

Moulin, C., Lambert, C. E., Poitou, J., and F. Dulac, 1996: Long term calibration of the Meteosat solar (VIS) channel using desert and ocean targets. *Int. J. Remote Sensing*, **17**, 1183-1200.

Moulin, C., and X. Schneider, 1999: Calibration of the Meteosat-5 sensor visible channel. *Int. J. Remote Sensing*, **20**, 195-200.

Rigollier, C., 2000: Vers un accès à une climatologie du rayonnement solaire : estimation de l'irradiation globale à partir d'images satellitales. Thèse de Doctorat, Université Nice – Sophia Antipolis, France, 194 p.

Rossow, W. B., Desormeaux, Y., Brest, C. L., and A. Walker (editors), 1992: International Satellite Cloud Climatology Project (ISCCP): Radiance calibration report. WMO/TD-No. 520, WCRP-77, World Climate Research Programme, International Council of Scientific Unions (ICSU) and World Meteorological Organisation (WMO), Geneva, December 1992, 104 pp.

Rossow, W. B., Brest, C. L., and M. D. Roiter, 1996: International Satellite Cloud Climatology Project (ISCCP), Update of radiance calibrations. WMO/TD-No. 736, World Climate Research Programme (ICSU and WMO), Geneva, 76 pp.

Schiffer, R.A., and W. B. Rossow, 1983: The International Satellite Cloud Climatology Project (ISCCP): The first project of the World Climate Research Programme. *Bull. Am. Meteor. Soc.*, **64**, 779-784.

Schiffer, R.A., and W. B. Rossow, 1985: ISCCP global radiance data set: A new resource for climate research. *Bull. Am. Meteor. Soc.*, **66**, 1498-1503.

Wald, L., 1989: Some examples of the use of structure functions in the analysis of satellite images of the ocean. *Photogramm. Eng. Remote Sensing*, **55**, 1487-1490.

Satellite	*Beginning of the period*		*End of the period*	
	Date	*Slot*	*Date*	*Slot*
Meteosat -1	9 December 1977		25 November 1979	
Meteosat -2	16 August 1981		11 August 1988	14
Meteosat -3	11 August 1988	17	19 June 1989	17
Meteosat -4	19 June 1989	18	24 January 1990	17
Meteosat -3	24 January 1990	19	19 April 1990	17
Meteosat -4	19 April 1990	19	30 October 1990	25
Meteosat -3	30 October 1990	27	5 November 1990	17
Meteosat -4	5 November 1990	19	11 December 1990	17
Meteosat -3	11 December 1990	19	13 December 1990	18
Meteosat -4	13 December 1990	20	22 January 1991	17
Meteosat -3	22 January 1991	18	25 January 1991	18
Meteosat -4	25 January 1991	19	2 May 1991	16
Meteosat -5	2 May 1991	18	3 May 1991	29
Meteosat -4	3 May 1991	30	26 November 1991	16
Meteosat -5	26 November 1991	19	29 November 1991	17
Meteosat -4	29 November 1991	18	11 February 1992	17
Meteosat -5	11 February 1992	19	5 February 1992	17
Meteosat -4	5 February 1992	19	8 September 1992	18
Meteosat -5	8 September 1992	19	24 September 1992	15
Meteosat -4	24 September 1992	16	4 May 1993	18
Meteosat -5	4 May 1993	19	7 May 1993	16

Meteosat -4	7 May 1993	18	3 November 1993	17
Meteosat -5	3 November 1993	21	18 November 1993	16
Meteosat -4	18 November 1993	20	4 February 1994	17
Meteosat -5	4 February 1994	19	21 October 1996	18
Meteosat -6	21 October 1996	19	25 October 1996	17
Meteosat -5	25 October 1996	18	13 February 1997	16
Meteosat -6	13 February 1997	18	3 June 1998	16
Meteosat -7	3 June 1998	17		

Table 1. History of the satellites of the Meteosat series, up to June 1998.

Meteosat-1	*Meteosat-2*	*Meteosat-3*	*Meteosat-4*	*Meteosat-5*	*Meteosat-6*	*Meteosat-7*
492.91	498.81	599.05	594.79	692.16	692.16	693.17

Table 2. Total irradiance I_{0met} in the visible channel for the various Meteosat sensors, in W m^{-2}.

Method	*Period*	*Number of samples*	*Mean (or bias)*	*RMSE*	*Correlation coefficient*
	1 Jan 1985 - 4 Feb 1994	3126	-	-	-
Moulin *et al.*		-	62.2	-	-
Present method		-	62.5	-	-
Difference		-	0.3 (0 %)	2.5 (4 %)	0.95
	1 Jan 1985 - 4 Feb 1994	1942	-	-	-
ISCCP		-	63.0	-	-
Present method		-	59.0	-	-
Difference		-	-4..0 (-6 %)	9.8 (16 %)	-
	1995 - 1997	1089	-	-	-
Govaerts *et al.*		-	82.1	-	-
Present method		-	77.7	-	-
Difference		-	-4.4 (5 %)	5.2 (6 %)	-

Table 3. Statistical results of the comparison of radiances (in W m^{-2} sr^{-1}) retrieved by the three identified concurrent methods and the present one for a numerical count of 100.

FIGURE CAPTIONS

Figure 1. Series of images available on 11 June 1996 in the B2 format. From left to right and top to bottom: slots 6, 12, 18, 24, 30, 36, 42, and 48.

Figure 2. Time series of the calibration coefficient a^t, in W m^{-2} sr^{-1} CN^{-1}, as a function of the number of Julian days after 6 Jan 1983.

Figure 3. Module of the Fourier transform of the timeseries of a^t for the interval [0, $0.01F_e$]. Dotted line represents the coefficient a^t computed from the original work of Lefèvre et al. (2000).

Figure 4. Time series of the coefficients a^{*t} as a function of the number of Julian days after 6 Jan 1983.

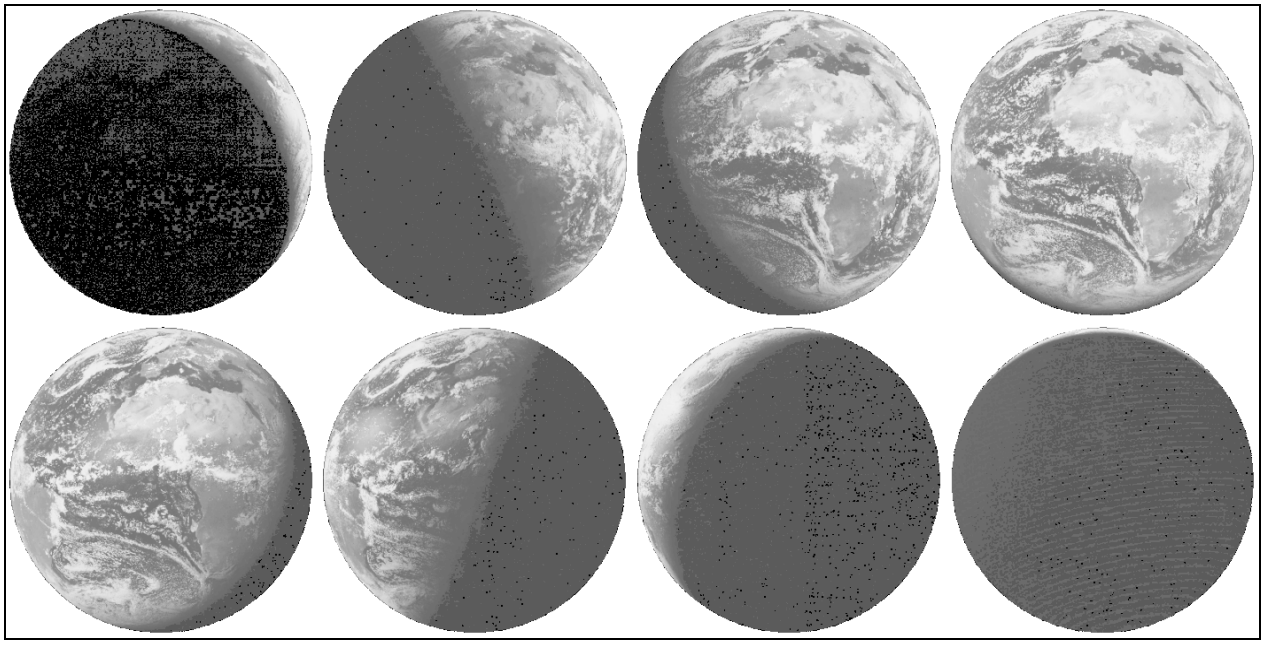

Figure 1.

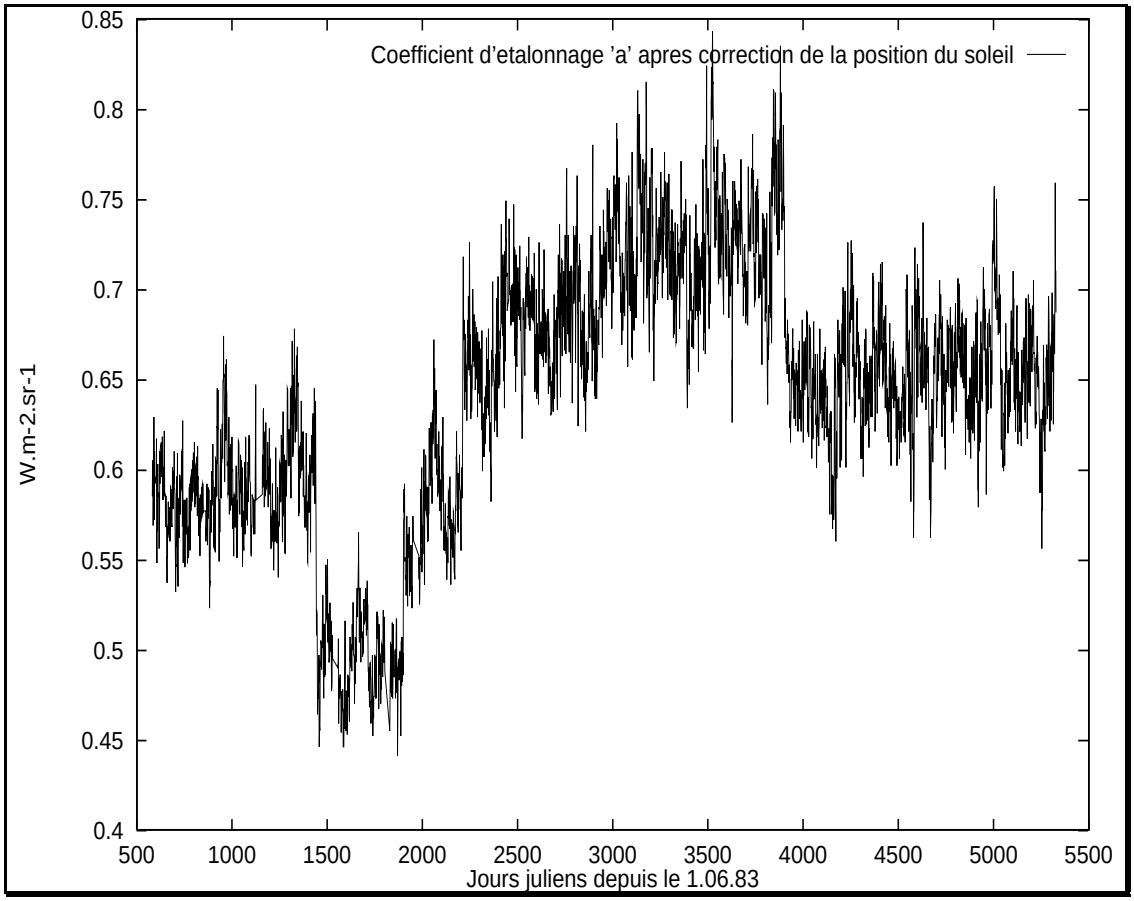

Figure 2. Time-series of the calibration coefficient a, in W m^{-2} sr^{-1} CN^{-1}, as a function of the number of days

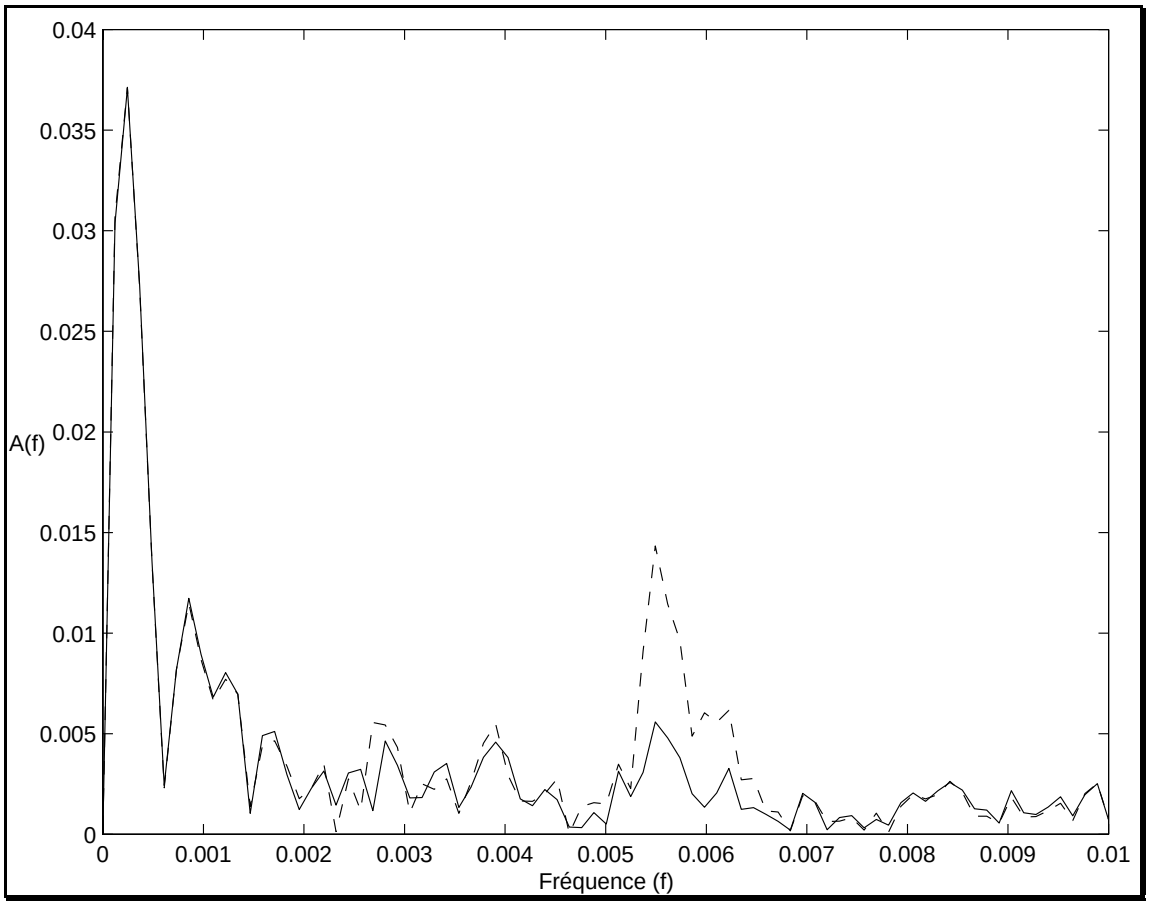

Figure 3. Module of the Fourier transform of the time-series of a for the interval [0, 0.01F_e]. Dotted line represents the coefficient a computed from the original work of Lefèvre et al.

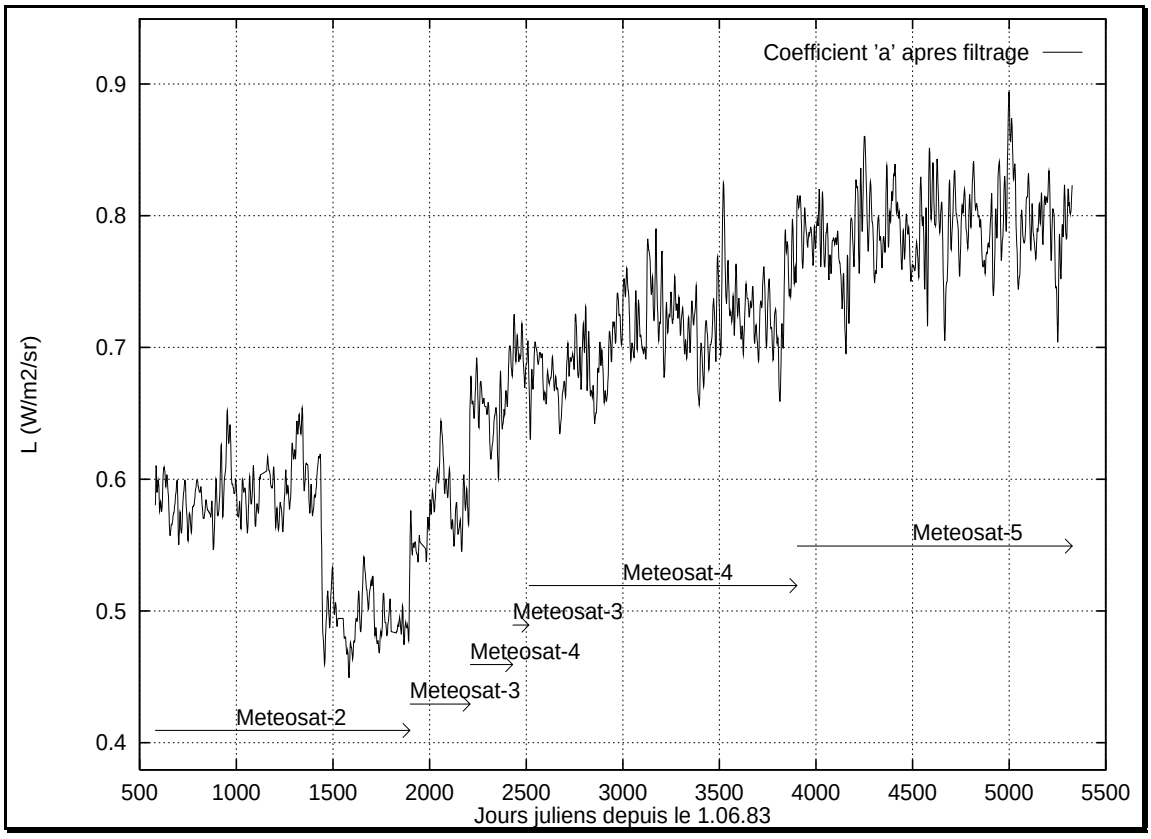

Figure 4. Time series of the coefficients a^{*t} as a function of the number of days